JOURNAL OF APPLIED CRYSTALLOGRAPHY

Volume 55 (2022)

Supporting information for article:

Structure refinement, microstrains and crystallite sizes of Mg-Ni-phyllosilicate nanoscroll powders

Aleksandr Levin, Ekaterina Khrapova, Daniil Kozlov, Andrei Krasilin and Victor Gusarov

Supporting information

S1. Rietveld refinement of structures of nanocrystalline Mg-Ni-phyllosilicate powders

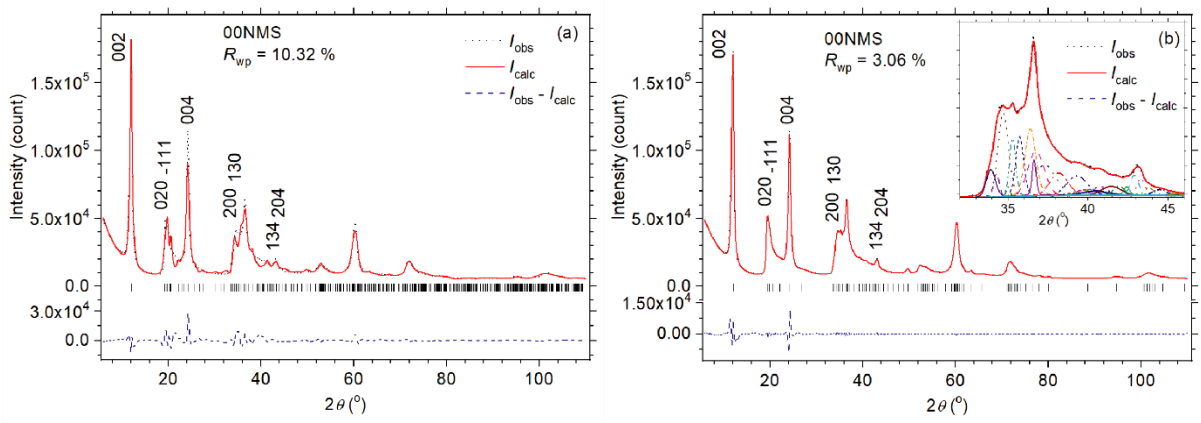

Figure S1 Experimental I_{obs}, calculated I_{calc} and difference $I_{obs} - I_{calc}$ XRD patterns of 00NMS powder sample according to results of Rietveld (a) and FP-profile peaks (b) fittings. Reached weight profile factor R_{wp} is shown. All theoretically possible 2θ angle positions of the reflections corresponding to refined unit cell parameters (a) or the 2θ angle positions of the reflections taken into account (b) are shown by vertical bars. The Miller indices hkl of the selected reflections, which give the main contribution to the observed reflections of the experimental XRD pattern, are indicated. Inset in (b) exhibit a part of XRD pattern in a selected 2θ range 32-46° in a larger scale and the contribution of extracted XRD reflections in the XRD pattern (each extracted reflection is presented together with contribution of background).

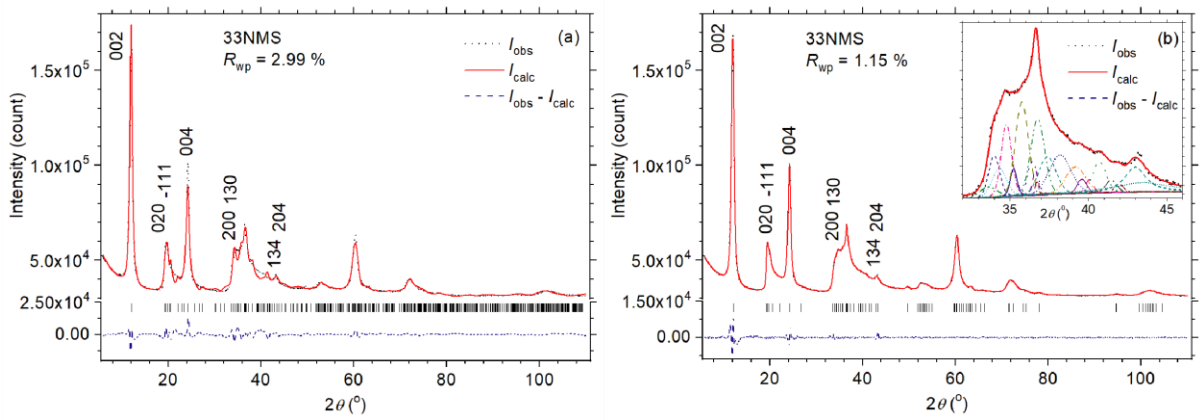

Figure S2 Same for 33NMS as in Fig. S1.

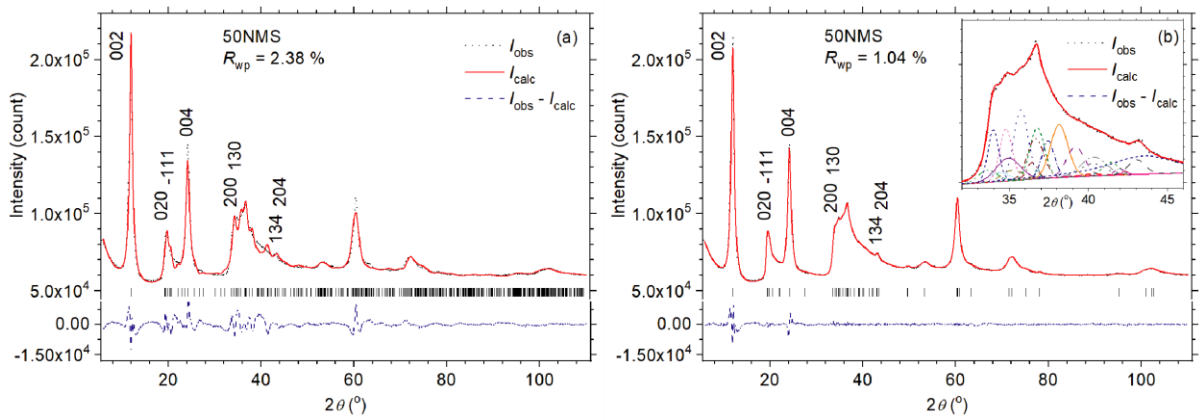

Figure S3 Same for 50NMS as in Fig. S1.

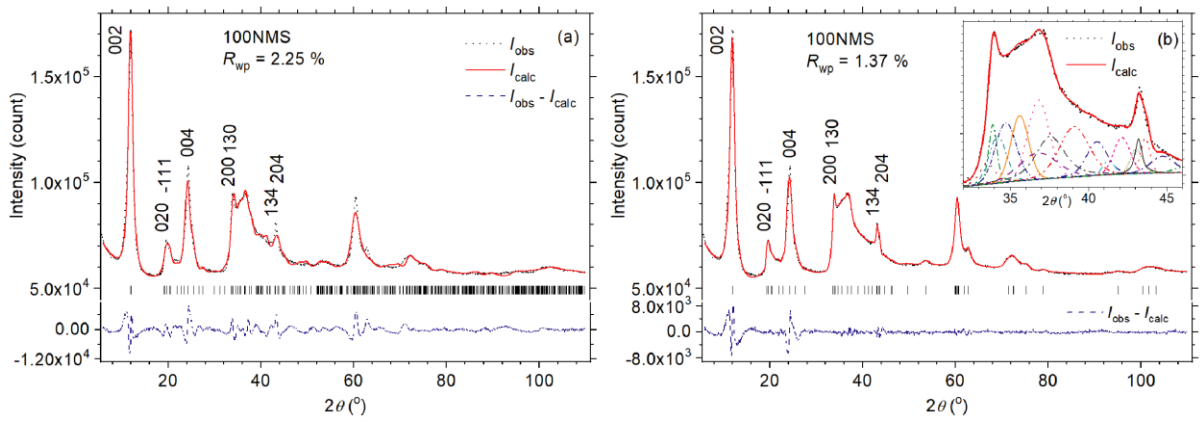

Figure S4 Same for 100NMS as in Fig. S1.

Table S1 Selected interatomic distances[a,b] (Å) in the structures $(Ni_xMg_{1-x})_3Si_2O_5(OH)_4$ according to results of the structure refinement by means of Rietveld method (Table 3 of paper), Me = Mg, Ni.

Atoms		0NMS-L	00NMS	33NMS	50NMS	67NMS	100NMS
Distances Me-O in MeO_6 octahedra							
$Me1$	O4	2.06(1)	2.06(2)	1.99(1)	1.99(2)	1.99(2)	1.99(2)
	O5	2.03(1)	2.07(1)	2.09(1)	2.11(2)	2.12(2)	2.11(2)
	O6	1.96(2)	1.92(1)	1.91(1)	1.90(2)	1.90(2)	1.89(2)
	O7	1.964(6)	1.89(2)	1.94(1)	1.90(2)	1.95(2)	1.94(1)
	O8	1.989(6)	2.02(1)	2.01(1)	2.01(1)	2.01(2)	2.00(1)
	O9	2.03(1)	2.09(1)	2.12(1)	2.13(2)	2.14(2)	1.96(2)
<$Me1$-O>		2.01(4)	2.01(8)	2.01(8)	2.01(10)	2.02(9)	1.98(7)
$Me2$	O4	2.041(9)	2.06(1)	2.07(1)	2.07(1)	2.07(2)	2.05(1)
	O5	2.08(1)	2.10(1)	2.10(1)	2.10(2)	2.12(2)	2.09(1)
	O6	2.018(7)	2.04(1)	2.09(1)	2.08(1)	2.09(2)	2.12(2)
	O7	1.95(1)	1.95(2)	2.10(1)	2.09(2)	2.07(3)	1.89(7)
	O8	1.98(1)	1.97(1)	1.94(1)	1.96(2)	1.96(2)	1.91(2)
	O9	2.03(1)	1.99(2)	2.04(1)	2.02(2)	1.99(2)	2.10(2)
<$Me2$-O>		2.02(4)	2.02(6)	2.06(6)	2.05(5)	2.05(6)	2.03(10)
$Me3$	O4	2.01(1)	1.98(2)	1.99(1)	2.00(2)	2.01(2)	2.00(2)
	O5	2.05(1)	2.07(1)	2.06(1)	2.04(1)	2.01(2)	2.04(1)
	O6	1.99(2)	1.90(1)	1.90(1)	1.89(2)	1.89(2)	1.89(2)
	O7	1.99(1)	2.09(2)	2.03(1)	1.98(2)	1.89(2)	2.04(2)
	O8	1.97(1)	1.90(2)	1.90(1)	1.89(2)	1.89(3)	1.89(3)
	O9	1.99(1)	1.94(1)	1.94(1)	1.93(1)	1.93(2)	2.02(2)
<$Me3$-O>		2.00(3)	1.98(8)	1.97(7)	1.96(6)	1.94(6)	1.98(7)
<Me-O>		2.01(4)	2.00(7)	2.01(8)	2.01(8)	2.00(8)	2.00(8)
Distances O-O in $Me1O_6$ octahedra							
O4	O5	2.98(1)	2.97(2)	2.90(2)	2.91(3)	2.93(3)	2.91(4)
	O6	2.64(1)	2.59(2)	2.55(1)	2.54(2)	2.55(3)	2.55(2)

	O7	2.53(1)	2.57(2)	2.69(1)	2.65(2)	2.69(3)	2.54(3)
	O8	3.118(8)	3.14(2)	3.06(2)	3.06(2)	3.07(3)	3.07(2)
	O7	2.55(2)	2.61(2)	2.59(1)	2.52(2)	2.50(3)	2.59(3)
O5	O8	3.127(9)	3.13(2)	3.14(2)	3.16(2)	3.17(3)	3.19(2)
	O9	2.80(2)	2.85(2)	2.90(1)	2.52(2)	2.89(3)	2.86(2)
	O7	3.13(1)	3.03(2)	3.08(2)	3.09(2)	3.16(3)	3.06(2)
O6	O8	2.34(2)	2.37(2)	2.37(1)	2.37(2)	2.37(3)	2.30(3)
	O9	2.98(2)	3.06(2)	3.07(2)	3.07(3)	3.08(3)	2.89(3)
O7	O9	3.231(8)	3.22(2)	3.17(2)	3.17(2)	3.20(3)	3.15(2)
O8	O9	2.40(1)	2.40(2)	2.41(1)	2.41(2)	2.38(3)	2.29(2)
<O-O>$_{Me1}$		2.82(32)	2.83(30)	2.83(29)	2.71(34)	2.83(32)	2.78(32)

Distances O-O in $Me2O_6$ octahedra

	O5	3.080(8)	3.08(2)	3.19(2)	3.19(2)	3.19(3)	3.18(2)
	O7	2.53(1)	2.57(2)	2.69(2)	2.65(2)	2.69(3)	2.54(3)
O4	O8	2.980(7)	3.01(2)	3.04(2)	3.04(2)	3.04(3)	3.02(2)
	O9	2.75(2)	2.69(2)	2.75(1)	2.75(2)	2.73(3)	2.88(2)
	O6	2.69(2)	2.64(2)	2.65(1)	2.62(2)	2.61(3)	2.62(3)
O5	O8	3.09(1)	3.08(2)	3.10(2)	3.08(3)	3.08(3)	3.07(4)
	O9	2.80(2)	2.85(2)	2.90(1)	2.92(2)	2.89(3)	2.86(2)
	O7	3.03(1)	3.13(2)	3.21(2)	3.22(2)	3.19(3)	3.07(2)
O6	O8	2.34(2)	2.37(2)	2.37(1)	2.37(2)	2.37(3)	2.30(3)
	O9	3.27(1)	3.27(2)	3.28(1)	3.29(2)	3.28(3)	2.89(3)
	O8	2.20(1)	2.32(2)	2.37(1)	2.33(2)	2.26(3)	2.18(2)
O7	O9	3.20(1)	3.04(3)	3.16(2)	3.18(3)	3.22(4)	3.15(2)
<O-O>$_{Me2}$		2.83(34)	2.84(31)	2.89(32)	2.88(34)	2.88(35)	2.81(33)

Distances O-O in $Me3O_6$ octahedra

	O5	3.186(8)	3.14(2)	3.09(2)	3.07(2)	3.06(3)	3.08(2)
O4	O6	2.64(1)	2.59(2)	2.55(1)	2.54(2)	2.55(3)	2.55(2)
	O8	3.22(1)	3.11(2)	3.16(2)	3.16(3)	3.16(3)	3.20(4)

	O9	2.75(2)	2.69(2)	2.75(1)	2.75(2)	2.73(3)	2.88(2)
O5	O6	2.69(2)	2.64(2)	2.65(1)	2.62(2)	2.61(3)	2.62(3)
	O7	2.55(2)	2.61(2)	2.59(1)	2.52(2)	2.50(3)	2.59(3)
	O8	3.099(9)	3.06(2)	3.03(2)	3.02(2)	3.02(3)	3.04(2)
O6	O7	3.09(2)	3.03(2)	2.90(2)	2.88(2)	2.83(3)	3.03(3)
	O9	3.01(1)	2.88(2)	2.86(1)	2.85(2)	2.85(3)	3.02(2)
O7	O8	2.20(1)	2.32(2)	2.37(1)	2.33(2)	2.26(3)	2.18(2)
	O9	2.856(8)	2.94(2)	2.87(2)	2.86(2)	2.79(3)	2.87(2)
O8	O9	2.40(1)	2.40(2)	2.41(1)	2.41(2)	2.38(3)	2.29(2)
<O-O>$_{Me3}$		2.81(33)	2.78(28)	2.77(26)	2.75(27)	2.73(28)	2.78(33)
<O-O>		2.82(32)	2.82(29)	2.83(29)	2.78(32)	2.81(31)	2.79(32)

Distances Si-O in SiO_4 tetrahedra

Si1	O1	1.675(9)	1.69(1)	1.68(1)	1.70(1)	1.69(2)	1.66(2)
	O2	1.658(9)	1.68(1)	1.70(1)	1.71(2)	1.70(3)	1.72(2)
	O3	1.666(7)	1.64(1)	1.68(1)	1.71(2)	1.73(2)	1.68(2)
	O4	1.69(2)	1.70(1)	1.70(1)	1.71(1)	1.70(2)	1.72(2)
<Si1-O>		1.67(1)	1.68(2)	1.69(1)	1.707(5)	1.71(2)	1.70(3)
Si2	O1	1.658(9)	1.63(1)	1.600(9)	1.61(1)	1.69(2)	1.70(2)
	O2	1.662(6)	1.63(1)	1.62(1)	1.61(2)	1.68(3)	1.69(2)
	O3	1.660(9)	1.69(1)	1.69(1)	1.69(2)	1.67(2)	1.67(2)
	O5	1.69(2)	1.70(1)	1.69(1)	1.71(2)	1.72(2)	1.71(2)
<Si2-O>		1.67(2)	1.66(4)	1.65(5)	1.66(5)	1.69(2)	1.69(2)
<Si-O>		1.67(1)	1.67(3)	1.67(4)	1.68(4)	1.70(2)	1.69(2)

Distances O-O in $Si1O_4$ tetrahedra

O1	O2	2.710(9)	2.70(1)	2.76(1)	2.77(2)	2.84(4)	2.87(2)
	O3	2.732(7)	2.72(1)	2.72(1)	2.74(2)	2.47(3)	2.41(2)
	O4	2.75(1)	2.81(2)	2.78(1)	2.82(2)	2.86(3)	2.86(3)
O2	O3	2.716(7)	2.71(2)	2.72(2)	2.74(2)	2.74(3)	2.72(3)
	O4	2.71(1)	2.80(2)	2.92(1)	2.95(2)	2.97(3)	2.98(3)

O3	O4	2.76(1)	2.72(2)	2.62(1)	2.67(2)	2.69(3)	2.64(2)
<O-O>$_{Si1}$		2.73(2)	2.74(5)	2.75(10)	2.78(10)	2.76(17)	2.75(20)
Distances O-O in $Si2O_4$ tetrahedra							
	O2	2.725(8)	2.68(1)	2.61(1)	2.59(2)	2.46(3)	2.41(2)
O1	O3	2.705(8)	2.65(1	2.64(1)	2.60(2)	2.84(3)	2.90(2)
	O5	2.74(1)	2.74(2)	2.70(1)	2.77(2)	2.87(3)	2.90(3)
	O3	2.717(7)	2.71(2)	2.73(1)	2.70(2)	2.72(3)	2.72(3)
O2	O5	2.71(1)	2.75(2)	2.78(1)	2.81(2)	2.85(3)	2.82(3)
O3	O5	2.73(2)	2.77(2)	2.69(1)	2.72(2)	2.77(3)	2.74(3)
<O-O>$_{Si2}$		2.72(1)	2.72(5)	2.69(6)	2.70(9)	2.75(15)	2.75(18)
<O-O>		2.73(2)	2.73(5)	2.72(8)	2.74(10)	2.76(16)	2.75(18)
Distances Me-Si in (MeO_6-SiO_4) double layers							
$Me1$	Si1	3.299(9)	3.337(9)	3.347(7)	3.360(9)	3.371(12)	3.367(9)
	Si2	3.298(7)	3.365(8)	3.354(7)	3.369(8)	3.410(12)	3.386(9)
$Me2$	Si1	3.278(9)	3.326(10)	3.201(8)	3.220(9)	3.244(13)	3.217(9)
	Si2	3.315(8)	3.354(11)	3.296(7)	3.326(9)	3.362(12)	3.374(10)
$Me3$	Si1	3.158(12)	3.184(10)	3.210(7)	3.218(9)	3.243(13)	3.243(11)
	Si2	3.177(9)	3.241(9)	3.242(8)	3.250(9)	3.213(15)	3.207(10)
<Me-Si>		3.25(7)	3.30(7)	3.28(7)	3.29(7)	3.31(8)	3.30(9)
Distances Me-Si between neighbouring (MeO_6-SiO_4) double layers							
$Me1$	Si1	5.103(4)	5.064(9)	5.050(7)	5.042(9)	5.022(13)	5.019(9)
	Si2	5.036(7)	4.964(8)	4.986(6)	4.966(8)	4.945(11)	4.948(9)
$Me2$	Si1	5.397(10)	5.003(9)	5.081(7)	5.047(9)	5.010(11)	4.996(9)
	Si2	5.408(6)	5.446(10)	5.399(10)	5.406(10)	5.358(17)	5.333(9)
$Me3$	Si1	4.836(12)	4.776(9)	4.786(6)	4.770(8)	4.755(12)	4.726(10)
	Si2	5.214(10)	5.204(10)	5.228(8)	5.231(9)	5.280(13)	5.183(11)

[a]The estimated standard deviations (e.s.d.s) of individual interatomic distances are calculated from the e.s.d.s of atomic coordinates (Table 3) and unit cell parameters (Table 2).

[b]The average distances in structural blocks given in angular brackets are obtained by the least-square averaging of the corresponding distances in these blocks.

S2. Estimation of microstrains

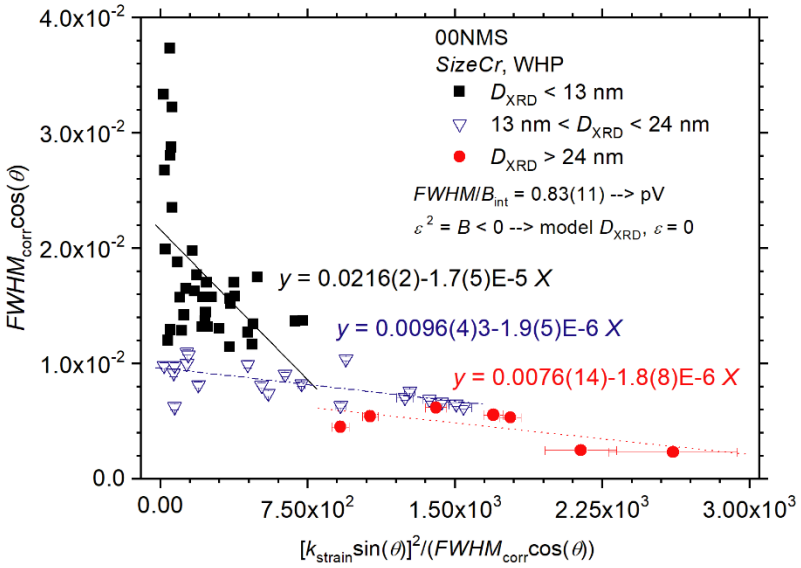

Figure S5 WHP (for reflections of pseudo-Voigt (pV) type) build for 00NMS sample. Fitting Williamson-Hall plots $y = A + BX$ are shown for three different ranges of crystallite sizes D_{XRD}, where $y = FWHM_{\mathrm{corr}}\cos(\theta)$, $X = [k_{\mathrm{strain}}\sin(\theta)]^2/(FWHM_{\mathrm{corr}}cos(\theta))$, $FWHM_{\mathrm{corr}}$ is $FWHM$ of reflection corrected to instrumental broadening, θ is half of the XRD reflection Bragg angle 2θ, $k_{\mathrm{strain}} = 4$

S3. Anisotropy of crystallites in the Rietveld fit of XRD patterns

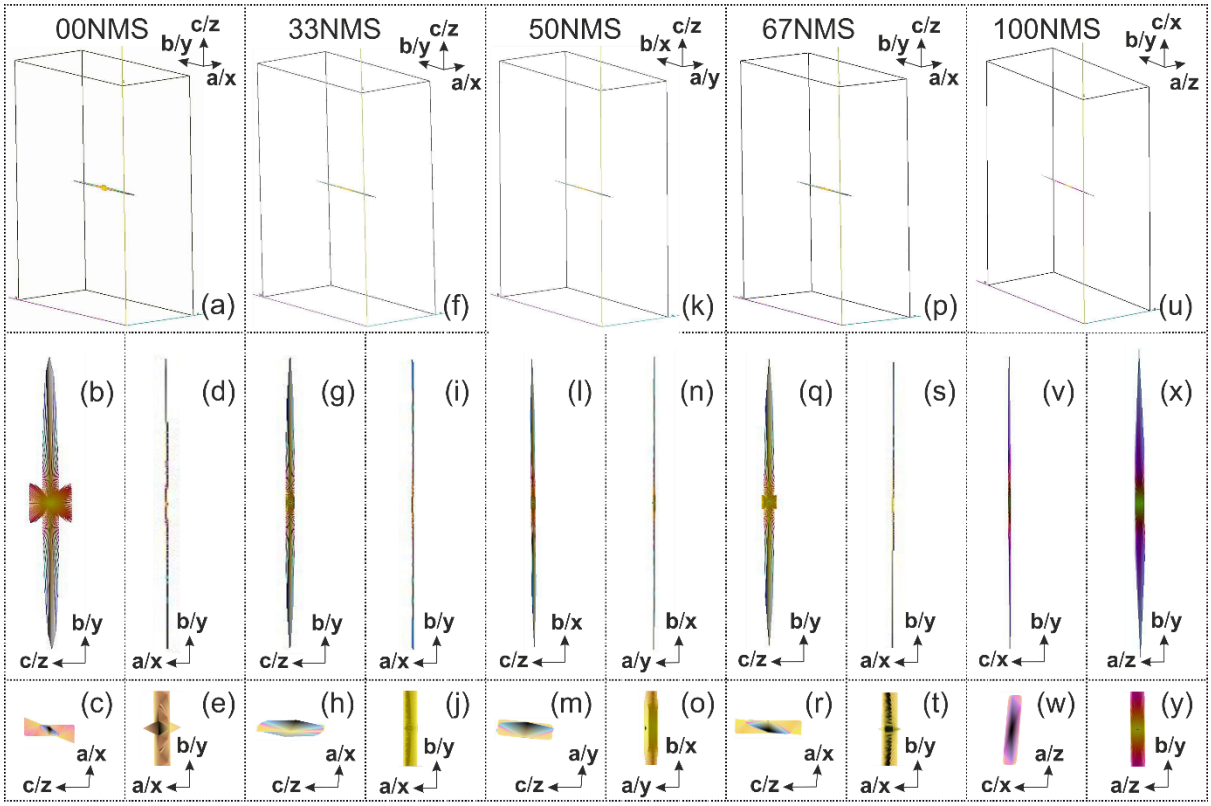

Figure S6 Shape of crystallites in the samples 00NMS ((a), (b), (c), (d), (e)), 33NMS ((f), (g), (h), (i), (j)), 50NMS ((k), (l), (m), (n), (o)), 67NMS ((p), (q), (r), (s), (t)) and 100NMS ((u), (v), (w), (x), (y)) for model $M = 1$ (needle-like plate ((110) for 100NMS and (011) for other compositions) elongated along [010]). In the top raw ((a), (f), (k), (p), (u)) the orientation of the crystallite in the unit cell is shown. In the first raw below, the projections of the crystallite to two main crystallographic planes ((011) in (b), (g), (j), (q) and (v) and (110) in (d), (i), (n), (s) and (x)) are shown. In the second raw below a projection on third main crystallographic plane (101) is shown in left columns ((c), (h), (m), (r) and (w)) in an enlarged scale and the right columns ((e), (j), (o), (t) and (y)) present the central part of the projection of the crystallite on the plane (110) in an enlarged scale. The direction of the axes of the unit cell (a, b, c) and axes of the modelled elliptic cylinder (x, y, z) are shown as well. The figures are given for qualitative consideration without observing the exact dimensions.

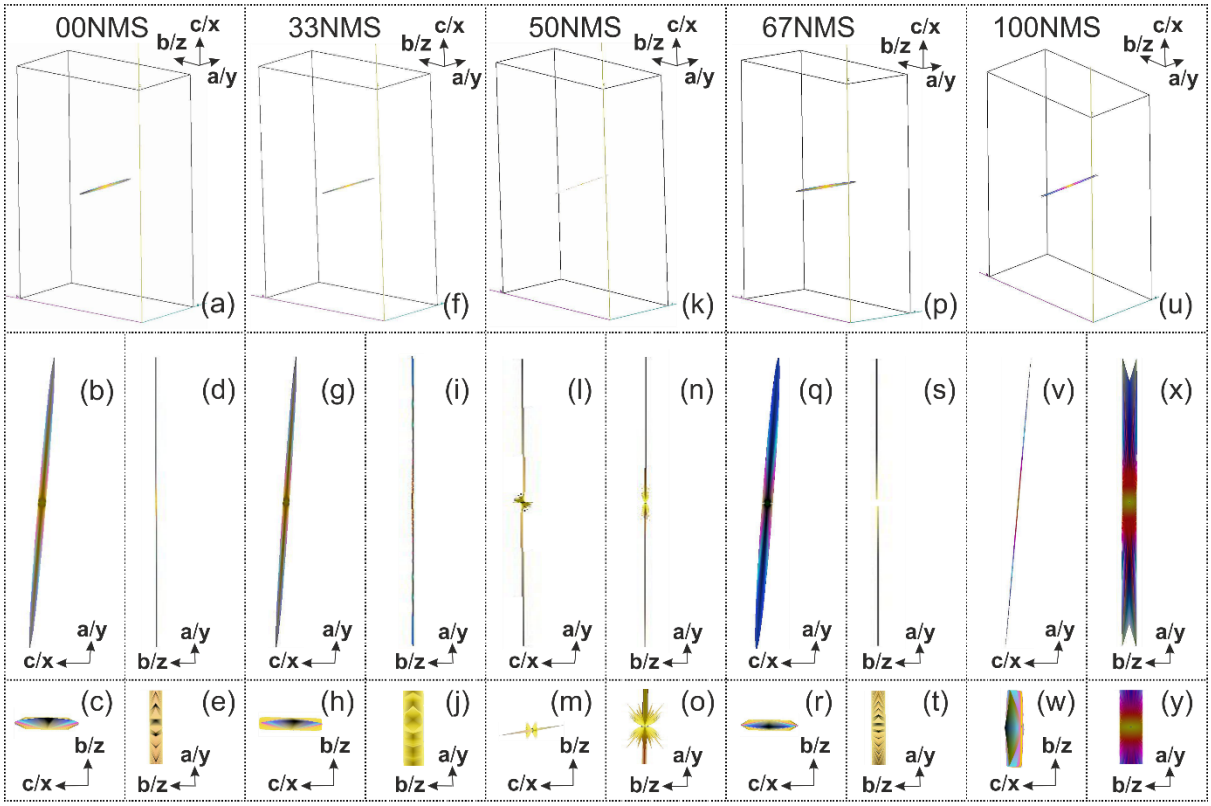

Figure S7 Shape of crystallites in the samples 00NMS ((a), (b), (c), (d), (e)), 33NMS ((f), (g), (h), (i), (j)), 50NMS ((k), (l), (m), (n), (o)), 67NMS ((p), (q), (r), (s), (t)) and 100NMS ((u), (v), (w), (x), (y)) for Model $M = 2$ (needle-like plate ((110) for 100NMS and (101) for other compositions) elongated along [100] or along crystallographic direction close to [100]). In the top raw ((a), (f), (k), (p), (u)) the orientation of the crystallite in the unit cell is shown. In the first raw below, the projections of the crystallite to two main crystallographic planes ((101) in (b), (g), (j), (q) and (v) and (110) in (d), (i), (n), (s) and (x)) are shown. In the second raw below a projection on third main crystallographic plane (011) is shown in left columns ((c), (h), (m), (r) and (w)) in an enlarged scale and the right columns ((e), (j), (o), (t) and (y)) present the central part of the projection of the crystallite on the plane (110) in an enlarged scale. The direction of the axes of the unit cell (a, b, c) and axes of the modelled elliptic cylinder (x, y, z) are shown as well. The figures are given for qualitative consideration without observing the exact dimensions.

S3.1. Alternative crystallite models

If the crystallite models $M = 1$ and $M = 2$ were obtained for all samples as a result of the refinement of the anisotropic sizes of the crystallites according to the procedure of (Estor *et al.*, 2015), then the model $M = 3$ gave acceptable results only for samples 00NMS, 33NMS, 67NMS and 100NMS. The crystallites in the model 3 ($M = 3$ in Table S2, Fig. S8) are similar to the cut-off version of the $M = 1$ crystallites. The radius of the base of the elliptical cylinder along [010] in this model is not as large as in the model $M = 1$, and ranges in different samples from ~771 to ~8787 nm. The second radius

(along [100] for samples 00NMS, 33NMS, and 67NMS, or along [001] for 100NMS) shows the smallest size ~12-13 nm for 00NMS, 33NMS, and 67NMS, and ~36 nm for 100NMS, which is very close to the sizes along the same directions in the $M = 1$ model. The third size (half the height of the elliptical cylinder along [001] for samples 00NMS, 33NMS, and 67NMS, or along [100] for 100NMS) shows a value also close to the corresponding sizes in the model $M = 1$ (~167-1184 nm for different samples). As a result, the crystallites in the model $M = 3$ can already be described in the first approximation, not as plate needles, but as usual plates (as in the model $M = 1$, with the orientation (011) relative to the crystallographic axes for samples 00NMS, 33NMS and 67NMS, and (101) for 100NMS), extended in the direction [010], see Fig. S8. In samples 00NMS, 33NMS and 67NMS, these plates are close to rectangular (with thickening in the central part in the case of samples 33NMS and 67NMS), and in the sample 100NMS have a halberd-like shape.

For the 100NMS sample, quite good results were also obtained when using the $M = 4$ crystallite model, which can be considered as an extension (variant) of the $M = 1$ model. In this model ($M = 4$ in Table S2, Fig. S9), the radius of the base of the elliptical cylinder along [010] has the largest size (~10000 nm, as in the model $M = 1$). The second radius (along [001]) has a size of ~43 nm, equal to half the height of the elliptical cylinder along [100] (in the $M = 4$ model, the relationship $R_{[100]\_\mathrm{surf}} = R_{[001]\_\mathrm{surf}}$ is superimposed during the refinement of the anisotropic sizes of the crystallite). As a result, the resulting shape of the crystallite in the first approximation can be considered as a needle-like parallelepiped-like column, elongated along the crystallographic direction [100] and narrowed at the ends, see Fig. S9.

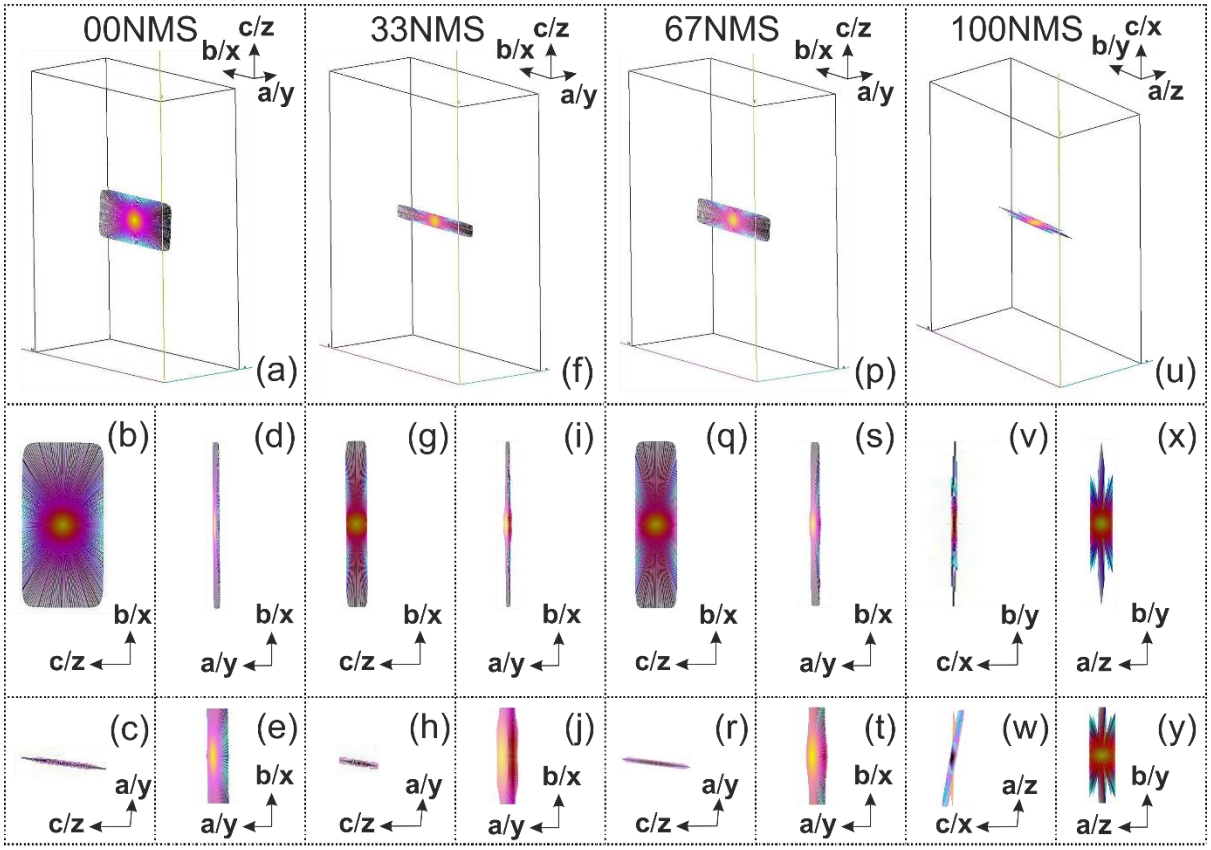

Figure S8 Shape of crystallites in the samples 00NMS ((a), (b), (c), (d), (e)), 33NMS ((f), (g), (h), (i), (j)), (o)), 67NMS ((p), (q), (r), (s), (t)) and 100NMS ((u), (v), (w), (x), (y)) for Model $M = 3$ (halberd-like (110) plate for 100NMS and rectangular (011) plate for other compositions, expanded along [010]). In the top raw ((a), (f), (p), (u)) the orientation of the crystallite in the unit cell is shown. In the first raw below, the projections of the crystallite to two main crystallographic planes ((011) in (b), (g), (q) and (v) and (110) in (d), (i), (s) and (x)) are shown. In the second raw below a projection on third main crystallographic plane (101) is shown in left columns ((c), (h), (r) and (w)) in an enlarged scale and the right columns ((e), (j), (t) and (y)) present the central part of the projection of the crystallite on the plane (110) in an enlarged scale. The direction of the axes of the unit cell (a, b, c) and axes of the modelled elliptic cylinder (x, y, z) are shown as well. The figures are given for qualitative consideration without observing the exact dimensions.

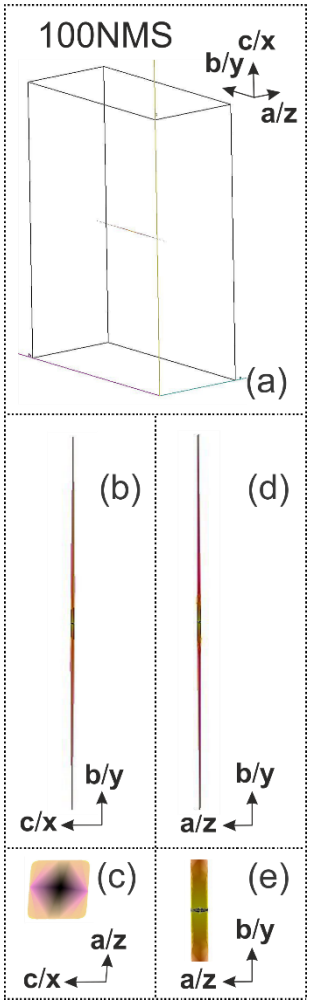

Figure S9 Shape of crystallites in the sample 100NMS for Model $M = 4$ (needle-like parallelepiped-like column with narrowed ends, expanded along [010]) elongated along [010]). In the top raw (a) the orientation of the crystallite in the unit cell is shown. In the first raw below, the projections of the crystallite to two main crystallographic planes ((011) in (b) and (110) in (d)) are shown. In the second raw below a projection on third main crystallographic plane (101) is shown in left column (c) in an enlarged scale and the right column (e) presents the central part of the projection of the crystallite on the plane (110) in an enlarged scale. The direction of the axes of the unit cell (a, b, c) and axes of the modelled elliptic cylinder (x, y, z) are shown as well. The figures are given for qualitative consideration without observing the exact dimensions.

Table S2 Parameters of crystallites in the elliptic cylinder models (with model number $M = 3$ and $M = 4$) obtained during the Rietveld refinement assuming anisotropic crystallite shape and quality R-factors of the refinement. Number of reflections $N_{\mathrm{refl}} = 454$ independent reflections in 2θ = 5.5-110°. Number of points in XRD patterns, N = 5140.

Sample	M	$R_{[100]\_\mathrm{surf}}$ (nm) $R_{[010]\_\mathrm{surf}}$ (nm)	τ_{XRD} $< \tau_{hkl} >$	μ σ	R_{wp} (%)	cR_{wp} (%) [g]	Elongated along	Shape in first approximation

		$R_{[001]\_surf}$ (nm)			R_p (%)	cR_p (%) [g]		
00NMS	3	12.3(1.3)[e] 771[a,e] 384[a,e]	2.00[a] 2.24(15)	3.92[b] 0.83[b]	10.08 7.50	19.44 17.99	[010]	Restangular (011) plate
33NMS	3	13.0(1.1)[e] 1126[a,e] 167[a,e]	2.00(1.66) 2.28(14)	3.79[b] 0.83[b]	2.93 2.03	13.92 16.45	[010]	Restangular (011) plate
67NMS	3	12.6(1.3)[e] 1160[a,e] 290[a,e]	2.00[a] 2.25(13)	3.97[b] 0.83[b]	2.62 1.79	15.30 17.35	[010]	Restangular (011) plate
100NMS	3	1184[a,f] 8787[a,f] 35.8(4.8)[f]	1.86[a] 2.09(13)	5.65[b] 0.79[b]	2.23 1.56	11.63 11.50	[010]	Halberd-like (110) plate
100NMS	4	42.6(5.7)[f] 10000[a,f] $R_{[100]\_surf}$ [f]	1.97[a] 2.53(30)	4.50[b] 0.82[b]	2.23 1.56	11.65 11.48	[010]	Needle-like parallelepiped-like column with narrowed ends

[a]E.s.d obtained during Rietveld refinement is larger than the refined value shown.

[b]Program does not show the e.s.d. of the parameter.

[e]Axes x, y, and z of the elliptic cylinder used for calculations of the crystallite shape are directed along [010], [100] and [001], respectively.

[f]Axes x, y, and z of the elliptic cylinder used for calculations of the crystallite shape are directed along [001], [010] and [100], respectively.

[g]Agreement factors provided by Rietveld program *TOPAS* were checked using manual calculations and the *RietESD* program. The presented agreement factors with subtraction of the background contribution are given in accordance with *RietESD* calculations (and manual ones).

S3.2. $L_{surf}(2\theta)$ distributions

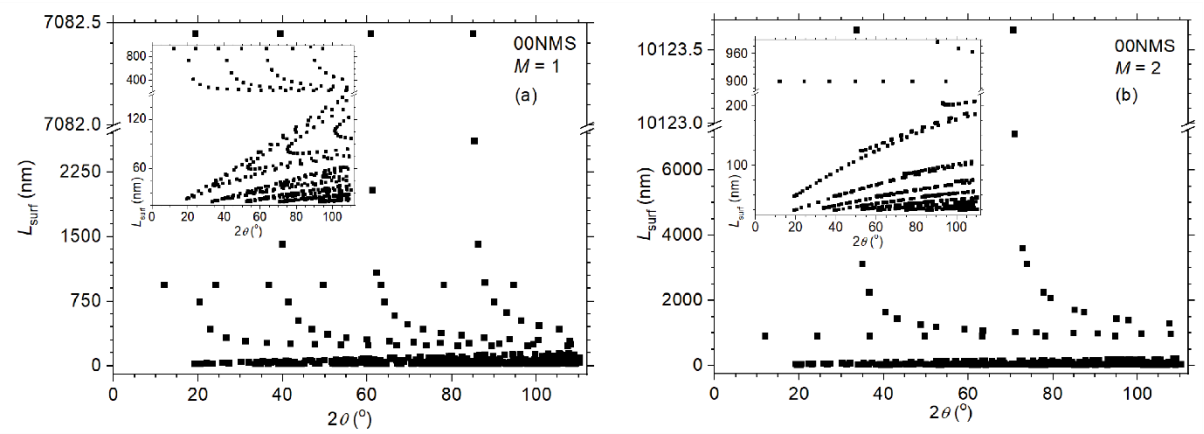

Figure S10 Sample 00NMS. Distribution of crystallite sizes L_{surf} in dependence on the Bragg angle 2θ of reflections obtained after Rietveld fitting taking into account the anisotropy of the crystallite sizes according to models $M = 1$ (a), $M = 2$ (b) (Fig. S6-S7, Table 4). The inset shows the distribution of small-sized crystallites on a larger scale.

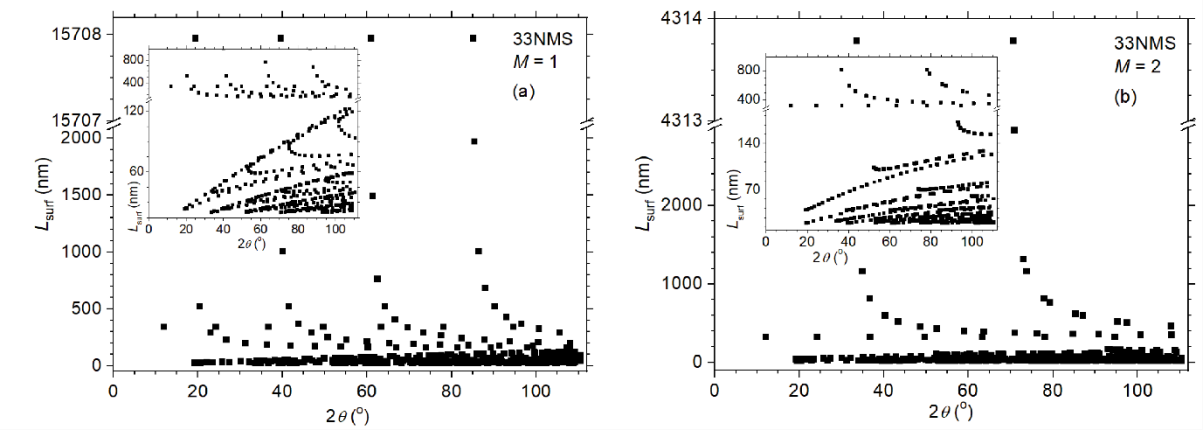

Figure S11 Sample 33NMS. Distribution of crystallite sizes L_{surf} in dependence on the Bragg angle 2θ of reflections obtained after Rietveld fitting taking into account the anisotropy of the crystallite sizes according to models $M = 1$ (a), $M = 2$ (b) (Fig. S6-S7, Table 4). The inset shows the distribution of small-sized crystallites on a larger scale.

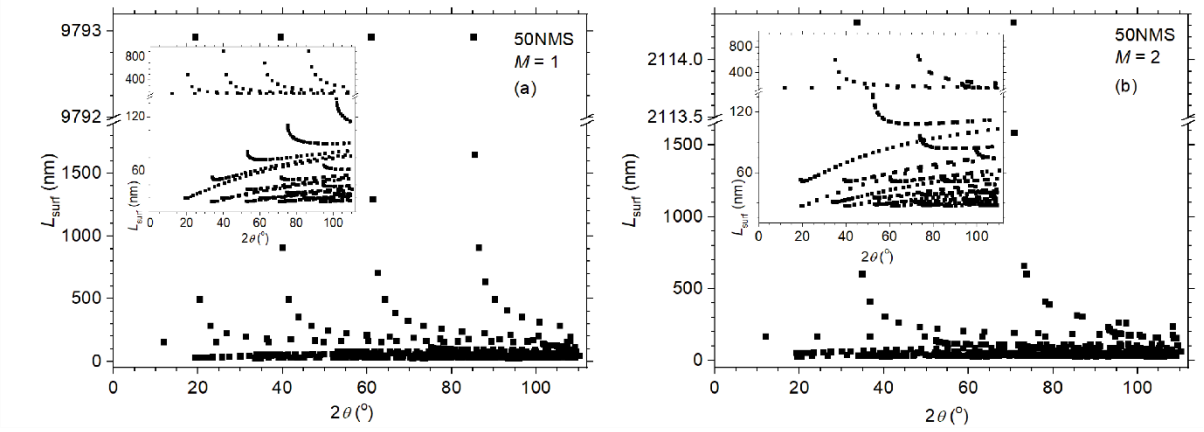

Figure S12 Sample 50NMS. Distribution of crystallite sizes L_{surf} in dependence on the Bragg angle 2θ of reflections obtained after Rietveld fitting taking into account the anisotropy of the crystallite sizes according to models $M = 1$ (a), $M = 2$ (b) (Fig. S6-S7, Table 4). The inset shows the distribution of small-sized crystallites on a larger scale.

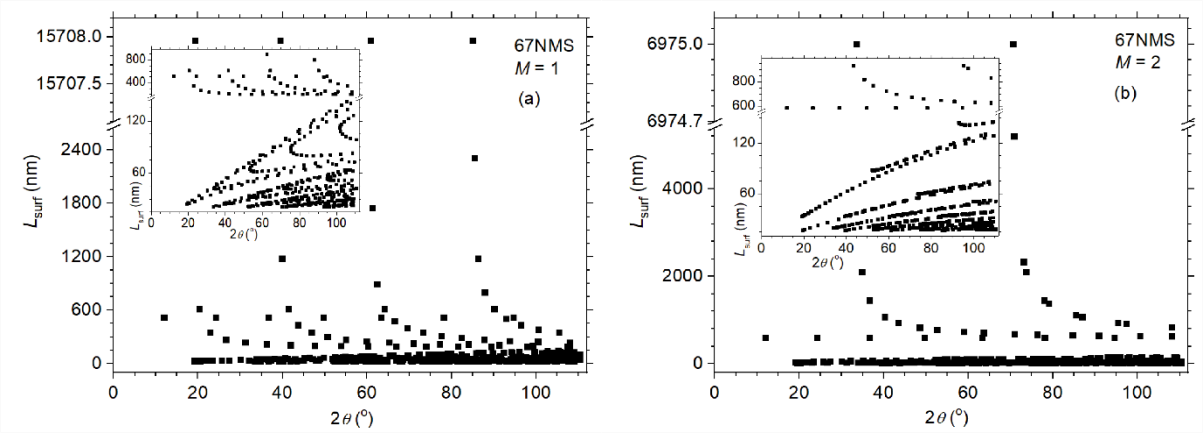

Figure S13 Sample 67NMS. Distribution of crystallite sizes L_{surf} in dependence on the Bragg angle 2θ of reflections obtained after Rietveld fitting taking into account the anisotropy of the crystallite sizes according to models $M = 1$ (a), $M = 2$ (b) (Fig. 7, Table 4). The inset shows the distribution of small-sized crystallites on a larger scale.

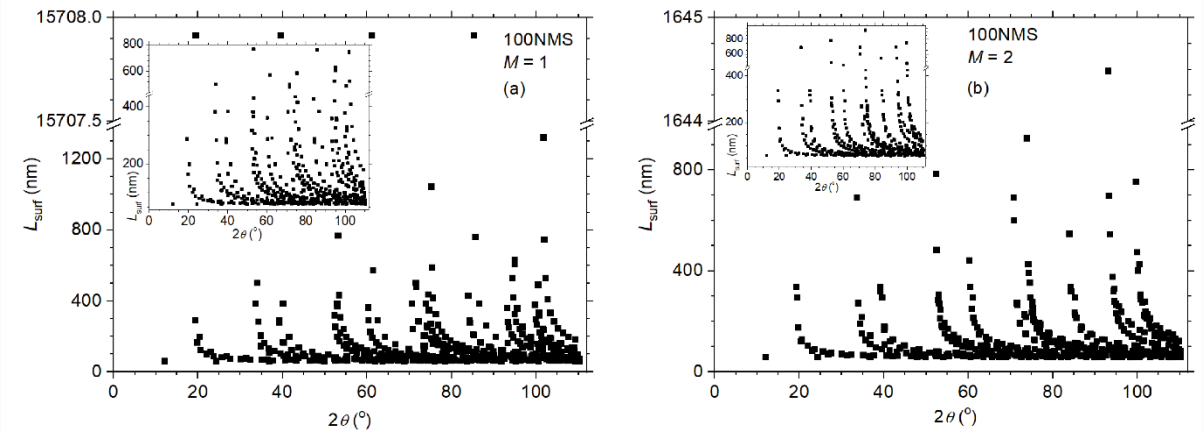

Figure S14 Sample 100NMS. Distribution of crystallite sizes L_{surf} in dependence on the Bragg angle 2θ of reflections obtained after Rietveld fitting taking into account the anisotropy of the crystallite sizes according to models $M = 1$ (a), $M = 2$ (b) (Fig. S6-S7, Table 4). The inset shows the distribution of small-sized crystallites on a larger scale.

S3.3. $L_{\mathrm{surf}}(\varphi)$ distributions

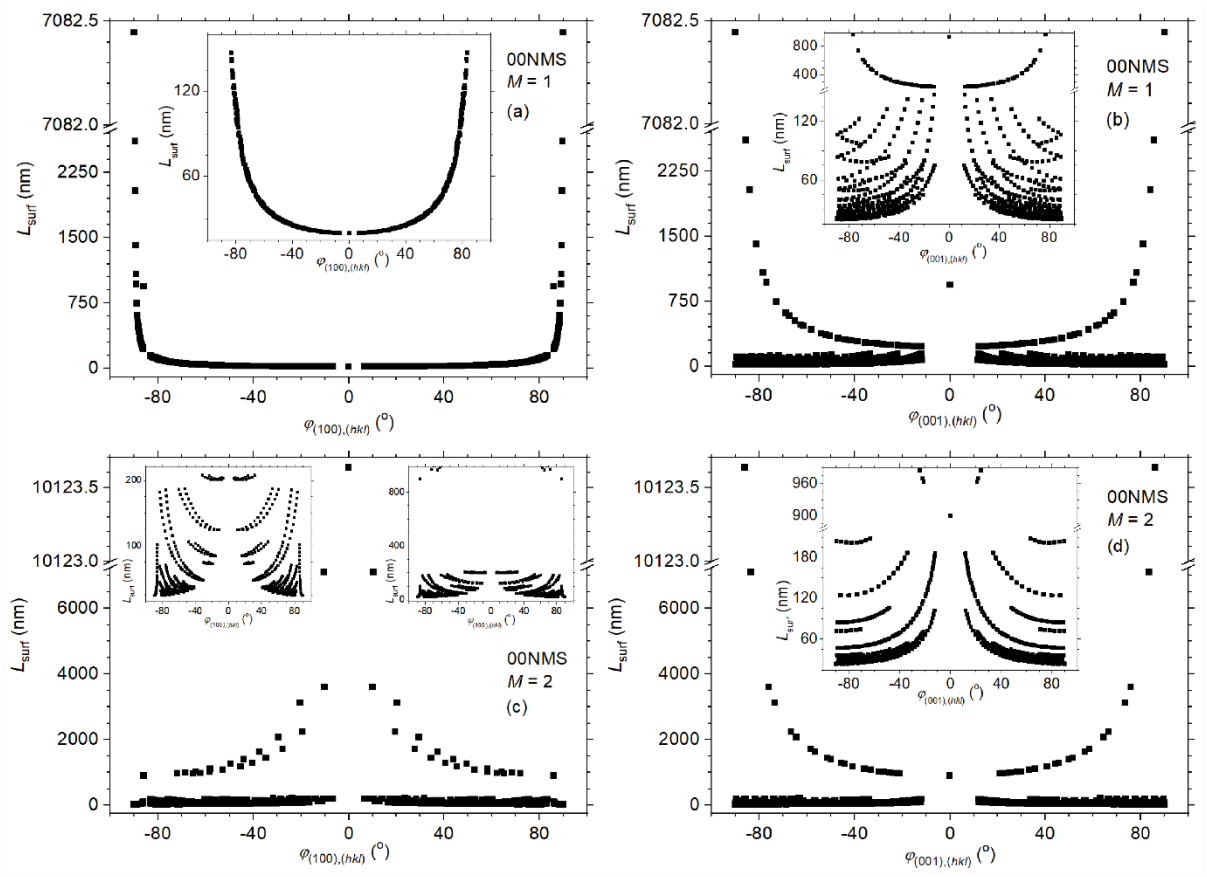

Figure S15 Sample 00NMS. Distribution of crystallite sizes L_{surf}, corresponding to reflections with Miller indices hkl versus angles φ between planes (hkl) and main crystallographic planes (100), (001) and (010) for the anisotropic crystallite models $M = 1$ (a, b) and $M = 2$ (c, d). Insets present the part of the distributions in a larger scale.

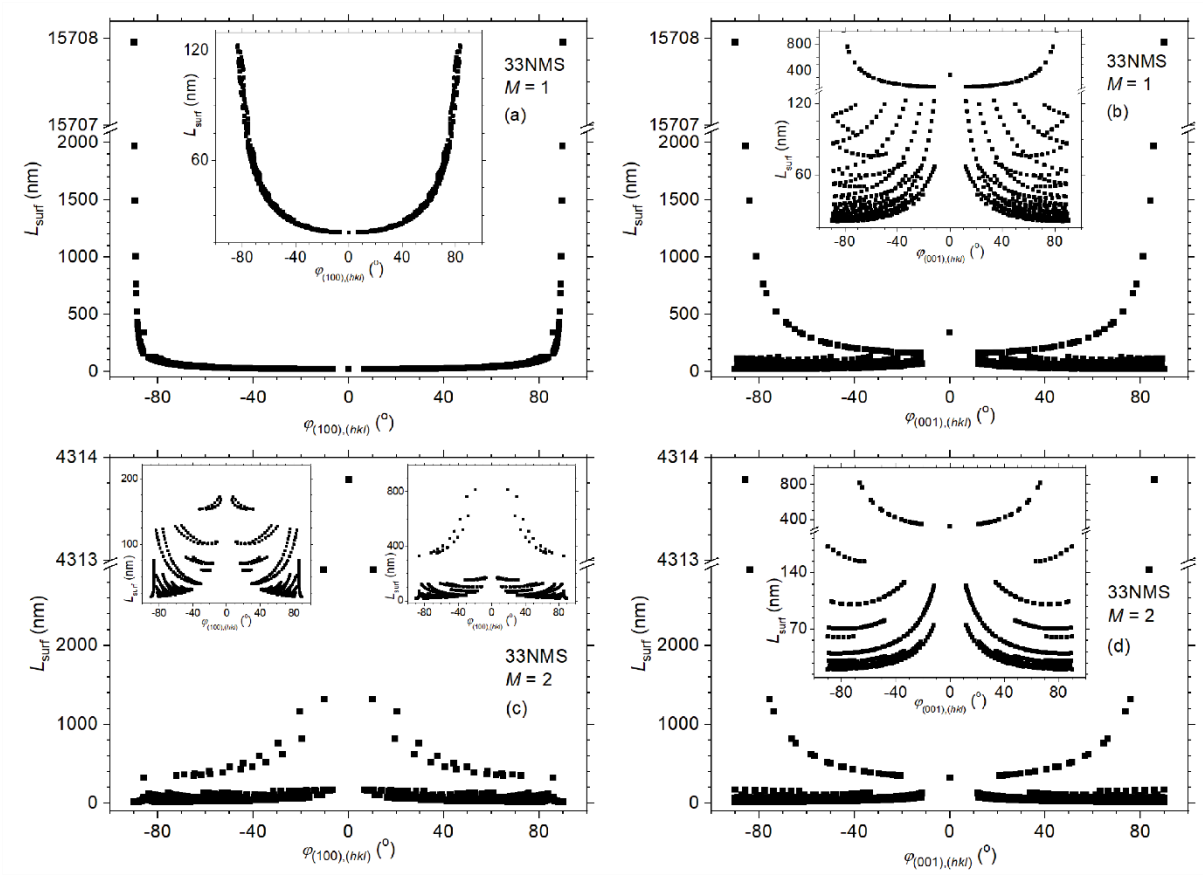

Figure S16 Sample 33NMS. Distribution of crystallite sizes L_{surf}, corresponding to reflections with Miller indices hkl versus angles φ between planes (hkl) and main crystallographic planes (100), (001) and (010) for the anisotropic crystallite models $M = 1$ (a, b) and $M = 2$ (c, d). Insets present the part of the distributions in a larger scale.

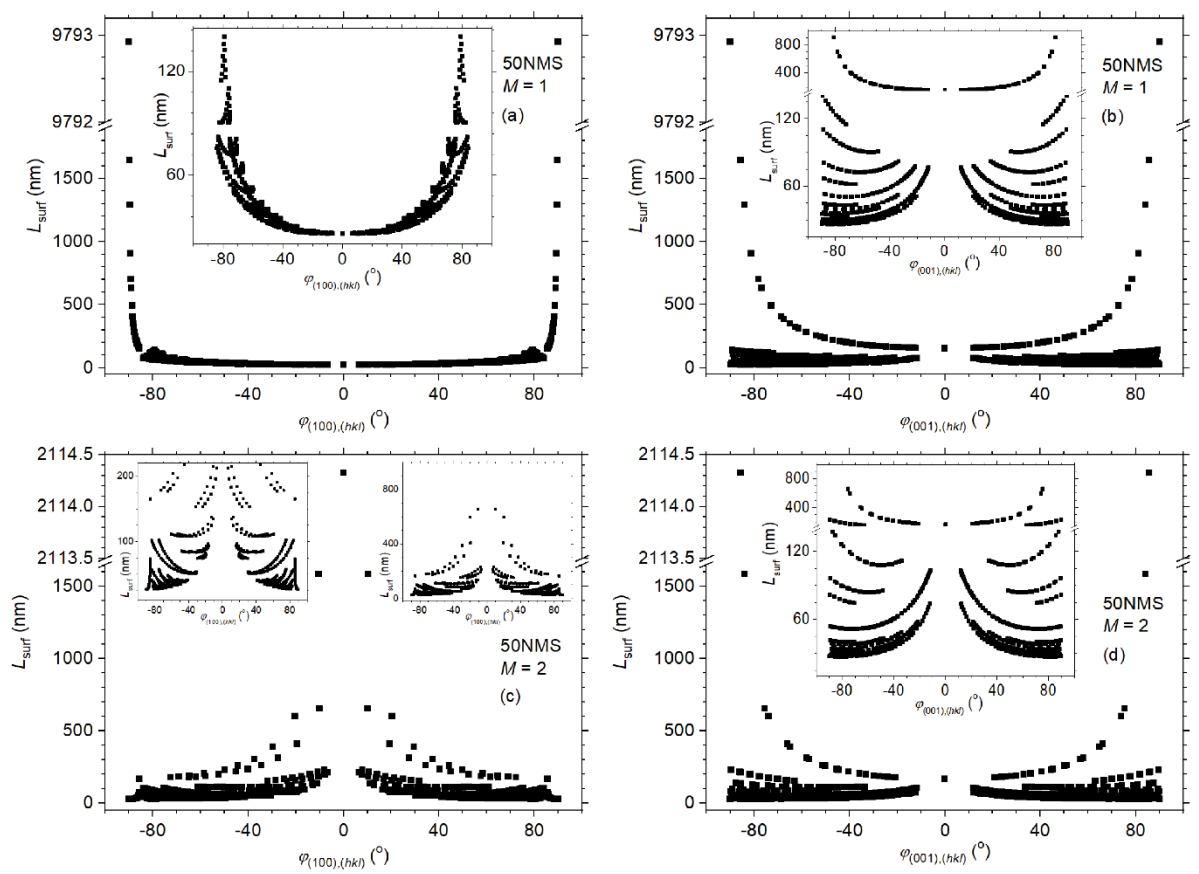

Figure S17 Sample 50NMS. Distribution of crystallite sizes L_{surf}, corresponding to reflections with Miller indices hkl versus angles φ between planes (hkl) and main crystallographic planes (100), (001) and (010) for the anisotropic crystallite models $M = 1$ (a, b) and $M = 2$ (c, d). Insets present the part of the distributions in a larger scale.

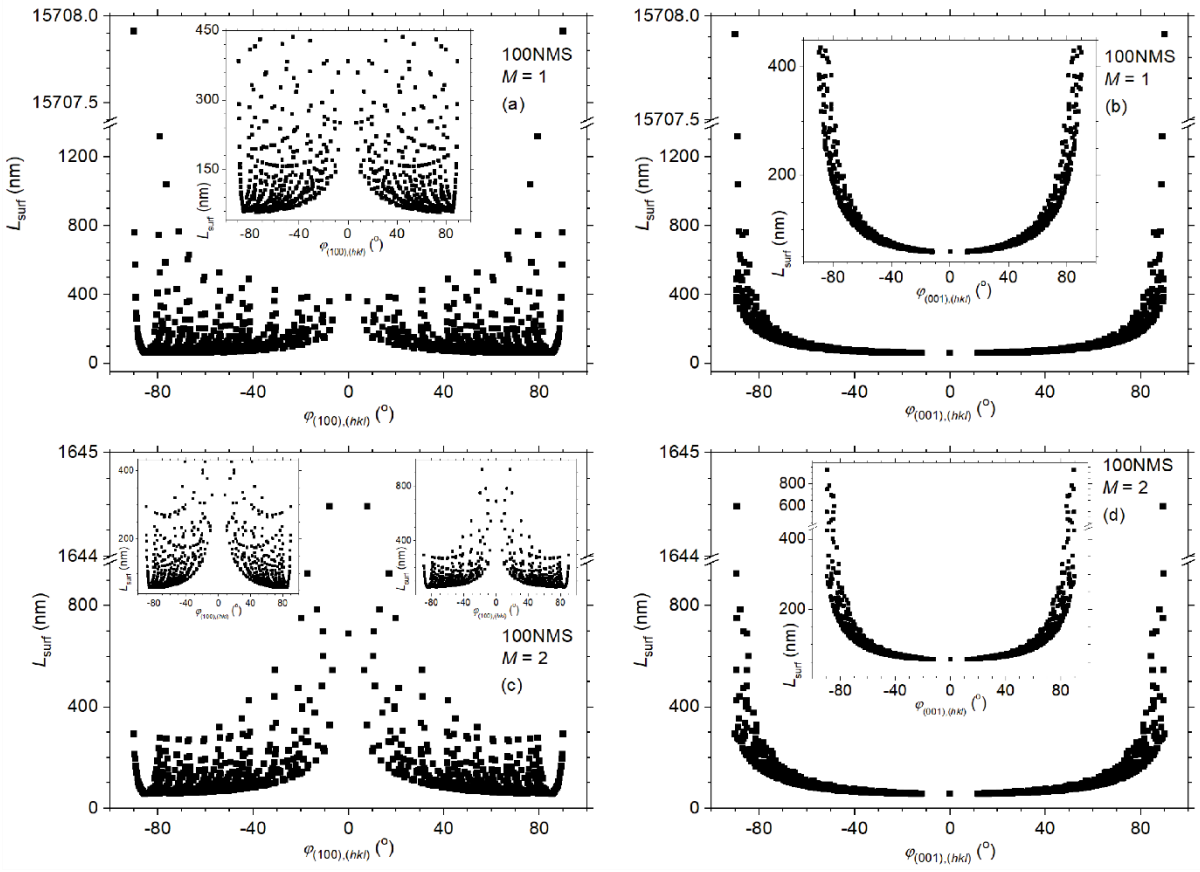

Figure S18 Sample 100NMS. Distribution of crystallite sizes L_{surf}, corresponding to reflections with Miller indices hkl versus angles φ between planes (hkl) and main crystallographic planes (100), (001) and (010) for the anisotropic crystallite models $M = 1$ (a, b) and $M = 2$ (c, d). Insets present the part of the distributions in a larger scale.

S4. Mean crystallite sizes and size distribution of crystallites based on the results of FP-profile fitting of XRD patterns by the Rietveld program *TOPAS*

S4.1. $D_{\mathrm{XRD}}(2\theta)$ distributions

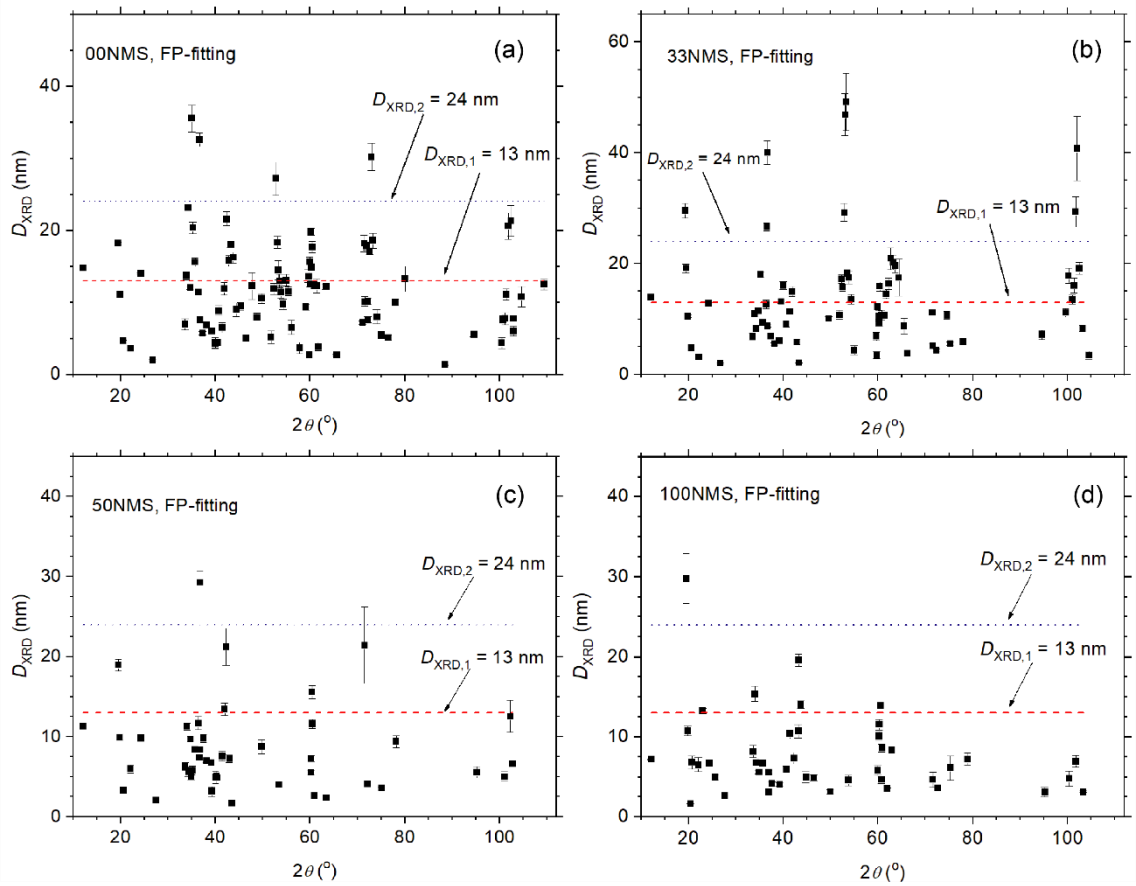

Figure S19 Samples 00NMS (a), 33NMS (b), 50NMS (c) and 100NMS (d). Sample 67NMS. Size D_{XRD} distribution of crystallites in dependence on the Bragg angle 2θ of reflections obtained after FP fitting. The characteristic limit sizes $D_{\mathrm{XRD},1} = 13$ nm and $D_{\mathrm{XRD},2} = 24$ nm used in the analysis are indicated.

S4.2. $D_{\mathrm{XRD}}(\varphi)$ distributions

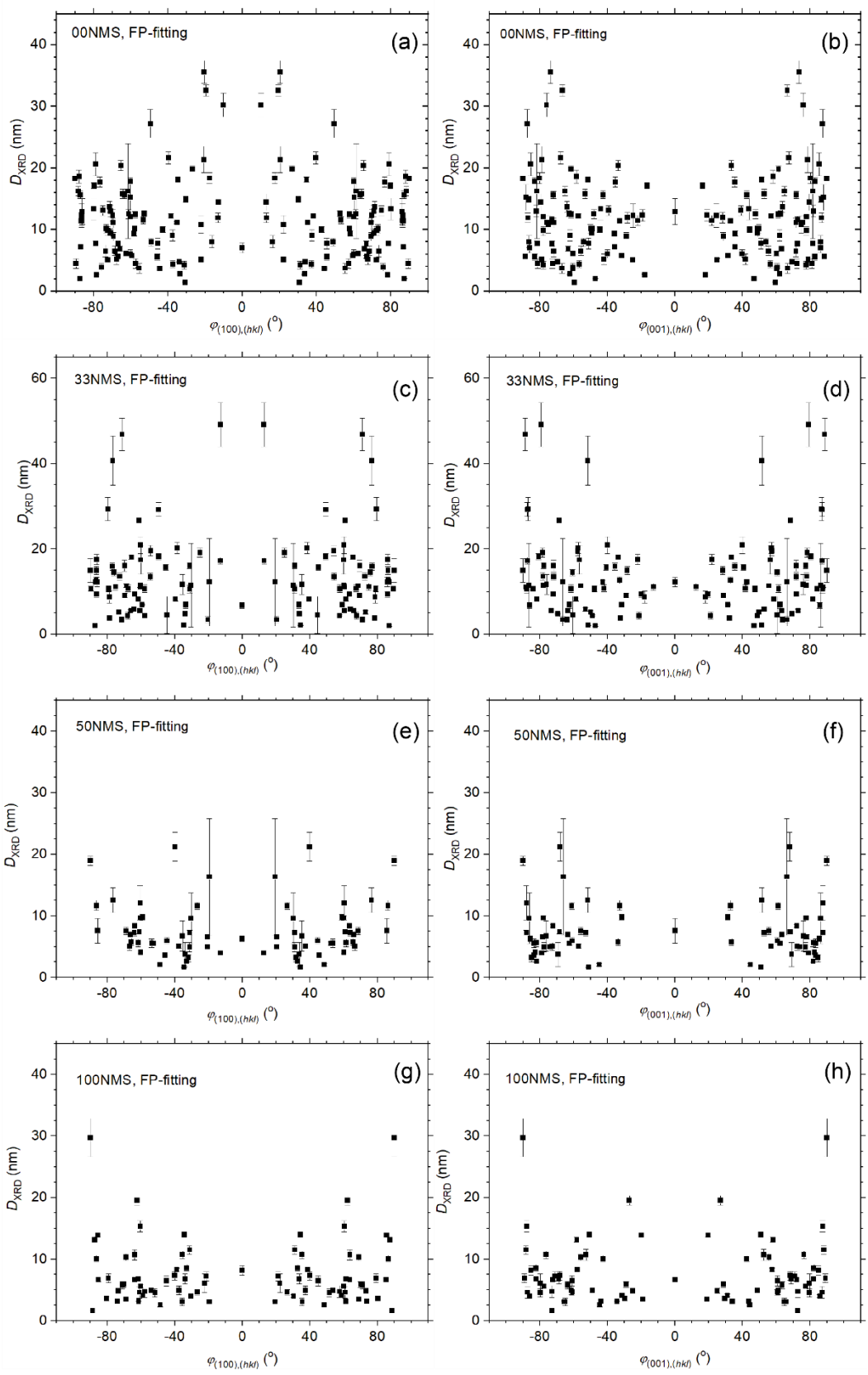

Figure S20 Distribution of the sizes D_{XRD} of crystallites in dependence on the angle φ between the crystallographic planes (hkl) and (100) (left column) or (001) (right column) for samples 00NMS (a,b), 33NMS (c,d), 50NMS (e,f), 100NMS (g,h).

S4.3. Average sizes of crystallites and size distribution of crystallites in the 67NMS powder according to results obtained by means of program *SizeCr*

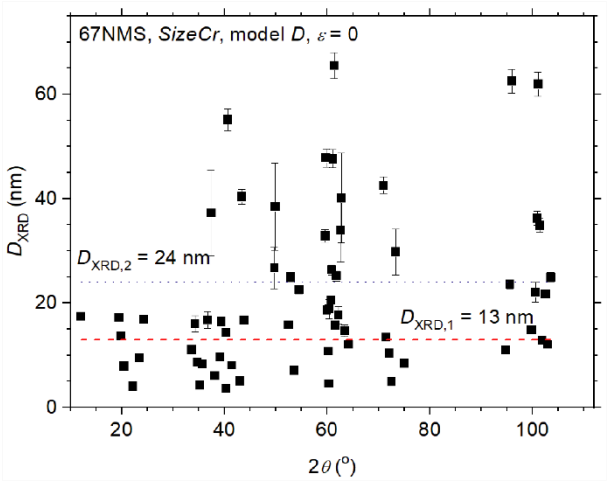

Figure S21 Sample 67NMS. Size D_{XRD} distribution of crystallites in dependence on the Bragg angle 2θ of reflections. The characteristic limit sizes $D_{\mathrm{XRD},1} = 13$ and $D_{\mathrm{XRD},2} = 24$ nm used in the analysis are indicated. Crystallite sizes D_{XRD} are obtained by means of program *SizeCr* (model D_{XRD}, $\varepsilon = 0$). Reflections are characterized by $D_{\mathrm{XRD}}/\sigma(D_{\mathrm{XRD}}) > 4/5$. $< D_{\mathrm{XRD}} >$ = 8.2(2.9) nm, 17.6(2.9) nm and 39.8(12.8) nm for $D_{\mathrm{XRD}} < 13$ nm, $13 < D_{\mathrm{XRD}} < 24$ nm and $D > 24$ nm, respectively.

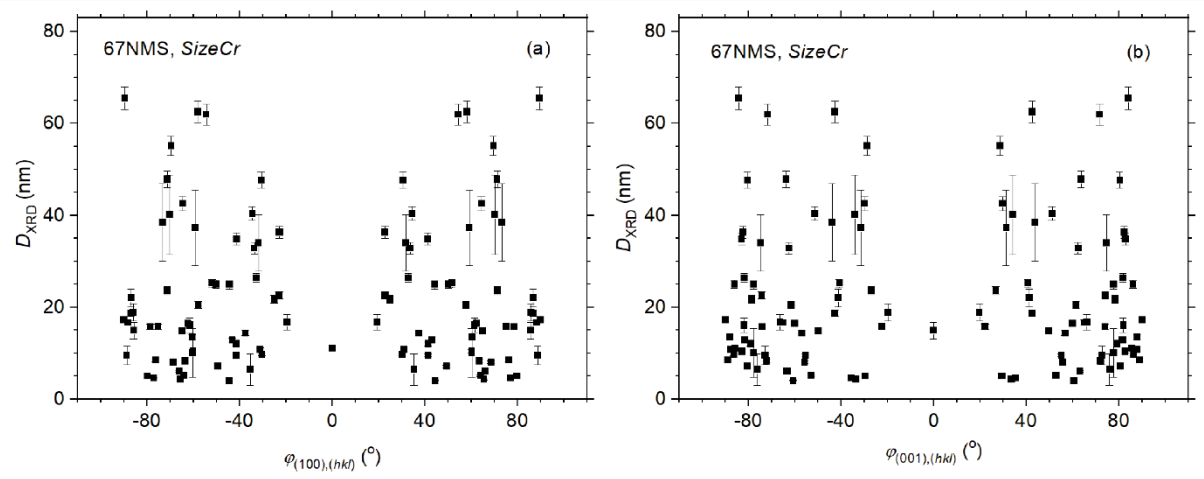

Figure S22 Sample 67NMS. Distribution of the sizes D_{XRD} of crystallites in dependence on the angle φ between the crystallographic planes (hkl) and (100) (a) and (001) (b). Reflections with Miller indices hkl, obtained after FP fitting method, and symmetrically related reflections with Miller indices $\bar{h}\bar{k}\bar{l}$ are used for distribution construction. Crystallite sizes D_{XRD} are obtained by means of program *SizeCr*. $< D_{[100]} >$ = 11.1(4) nm, $< D_{[001]} >$ = 14.9(1.8) nm, $< D_{[010]} >$ = 17.2(6) nm.

S5. TEM size distributions and SEM micrographs

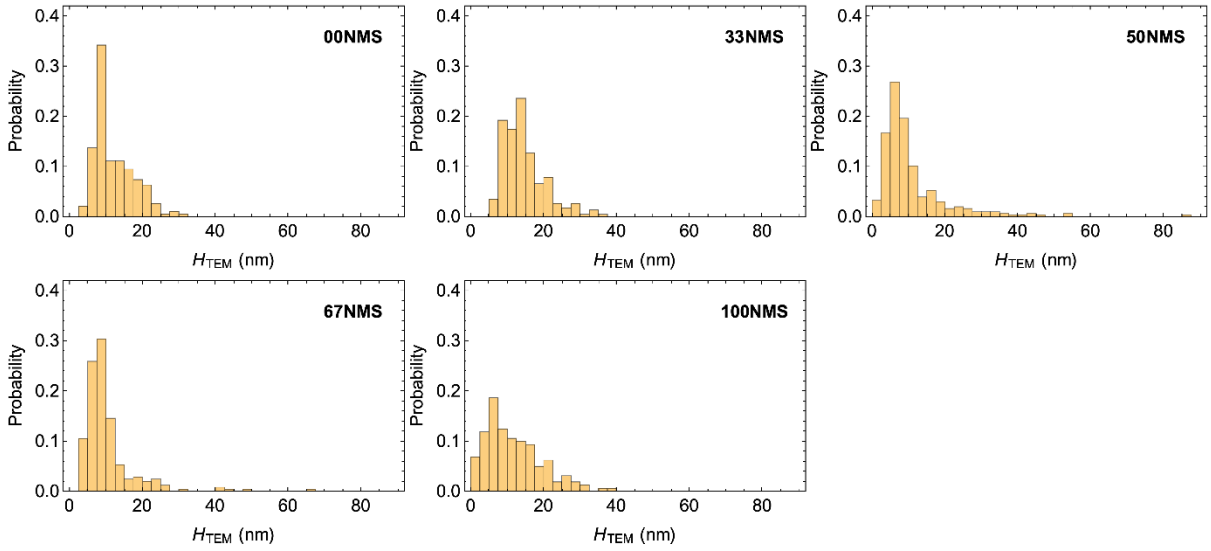

Figure S23 Nanoscrolls wall thickness distribution measured by TEM.

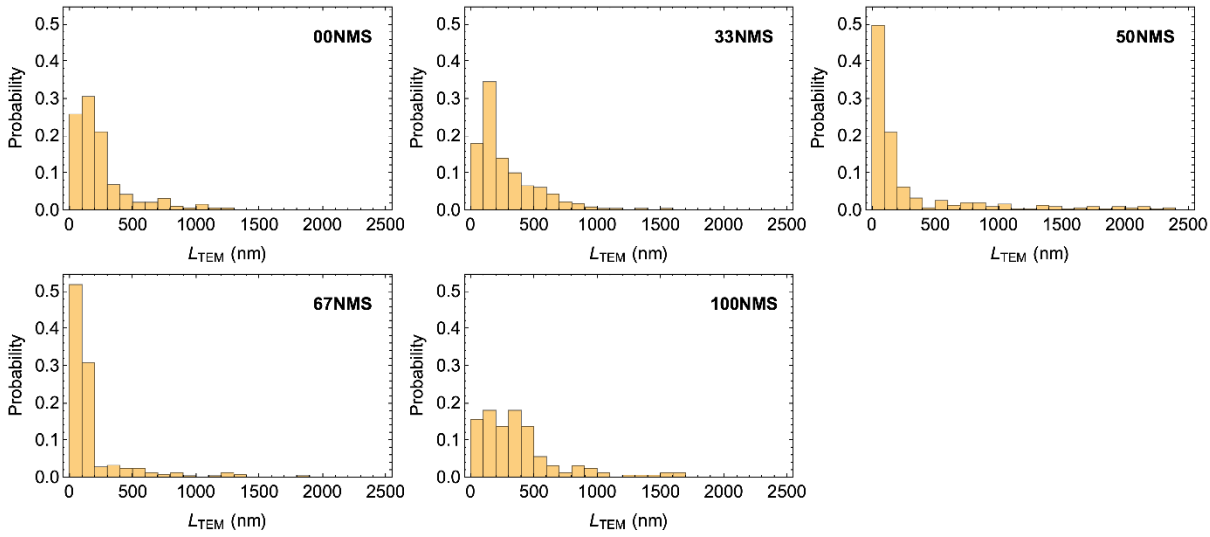

Figure S24 Nanoscrolls length distribution measured by TEM.

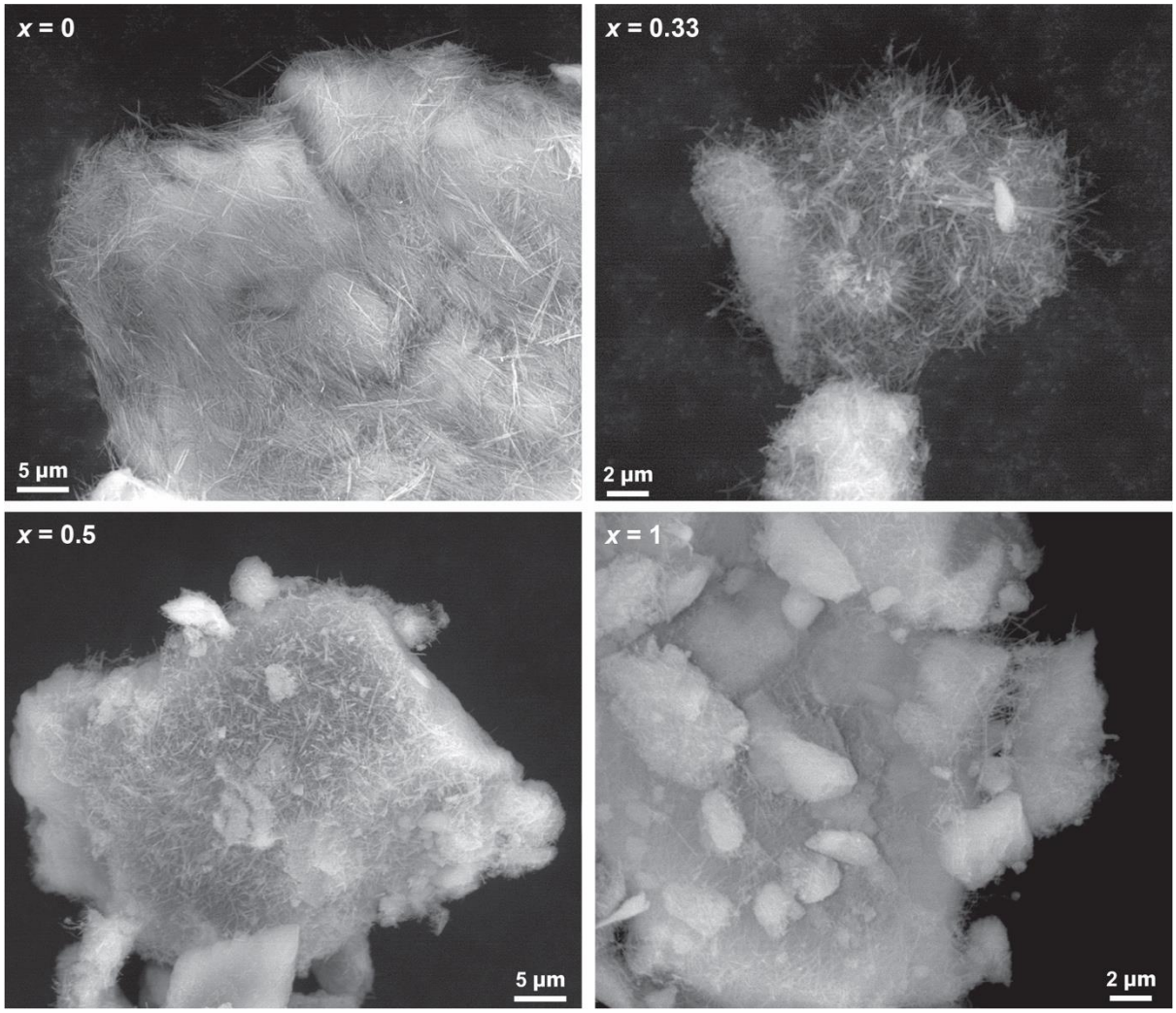

Figure S25 SEM images of $(Ni_xMg_{1-x})_3Si_2O_5(OH)_4$ nanoscrolls aggregates.